

Harter, T., E.R. Atwill, L.L. Hou, B.M. Karle, and K.W. Tate, 2008.
 Developing risk models of *Cryptosporidium* transport in soils from
 vegetated, tilted soilbox experiments. *J. Env. Qual.* 37(1), 245-258.
 doi:10.2134/jeq2006.0281.

Developing Risk Models of *Cryptosporidium* Transport in Soils from Vegetated, Tilted Soilbox Experiments

Thomas Harter,* Edward R. Atwill, Lingling Hou, Betsy M. Karle, and Kenneth W. Tate University of California—Davis

Transport of *Cryptosporidium parvum* through macroporous soils is poorly understood yet critical for assessing the risk of groundwater contamination. We developed a conceptual model of the physics of flow and transport in packed, tilted, and vegetated soilboxes during and immediately after a simulated rainfall event and applied it to 54 experiments implemented with different soils, slopes, and rainfall rates. Using a parsimonious inverse modeling procedure, we show that a significant amount of subsurface outflow from the soilboxes is due to macropore flow. The effective hydraulic properties of the macropore space were obtained by calibration of a simple two-domain flow and transport model that accounts for coupled flow in the matrix and in the macropores of the soils. Using linear mixed-effects analysis, macropore hydraulic properties and oocyst attenuation were shown to be associated with soil bulk density and rainfall rate. Macropore flow was shown to be responsible for bromide and *C. parvum* transport through the soil into the underlying pore space observed during the 4-h experiments. We confirmed this finding by conducting a pair of saturated soil column studies under homogeneously repacked conditions with no macropores in which no *C. parvum* transport was observed in the effluent. The linear mixed-effects and logistic regression models developed from the soilbox experiments provide a basis for estimating macropore hydraulic properties and the risk of *C. parvum* transport through shallow soils from bulk density, precipitation, and total shallow subsurface flow rate. The risk assessment is consistent with the reported occurrence of oocysts in springs or groundwater from fractured or karstic rocks protected only by shallow overlying soils.

THE occurrence of the protozoal pathogen *Cryptosporidium parvum* in drinking water sources is recognized as a significant threat to private and public water supplies throughout the world (Rose et al., 1991; Lisle and Rose, 1995; Messner and Wolpert, 2000). *Cryptosporidium parvum* can be isolated from animal and human sources, with this species of *Cryptosporidium* along with *C. hominis* functioning as the primary etiologic agents of human cryptosporidiosis. The oocyst, which is the infectious and environmentally disseminated stage of *C. parvum*, is relatively resistant to a variety of commonly used water treatment procedures, such as chlorination. Hence, understanding the occurrence, fate, and transport of *C. parvum* in watersheds, surface water, and groundwater is critical in developing control strategies that reduce the risk of *C. parvum* in drinking water sources.

Environmental pathways for transporting a terrestrial load of *C. parvum* oocysts to drinking water sources include the runoff-surface water route, the infiltration-interflow-surface water route, the infiltration-groundwater-tile drain-surface water route, and the infiltration-groundwater-drinking water well route (Atwill, 1996; Walker et al., 1998; Harter et al., 2000). One of the least understood hydrologic pathways of *C. parvum* is the transmission through soils and the unsaturated zone immediately after infiltration (Bradford and Schijven, 2002). Soil transmission occurs from the land surface to groundwater (recharge) or from the land surface via lateral flow in the unsaturated zone to low-order streams or back to the land surface (interflow). Soil passage is generally considered an insignificant component of the total oocyst transport through a watershed (e.g., Walker and Stedinger, 1999). The occurrence of *C. parvum* in tile drain discharge and in groundwater of highly fractured consolidated formations or coarse-grained unconsolidated formations, however, indicates that the unsaturated zone plays a potentially significant role in assessing the risk of *C. parvum* transmission to tile drains, groundwater resources, and potentially in hillslope flow processes (Amirtharajah et al., 2002; Bicu-do and Goyal, 2003; De Carvalho et al., 2000; Moulton-Hancock et al., 2000; Morris and Foster, 2000; Svoboda et al., 1999).

For saturated transport in packed sandy soils or in glass bead porous media, the conceptual framework of transport by advection-dispersion, dynamic sorption, and permanent filtration due to

Copyright © 2008 by the American Society of Agronomy, Crop Science Society of America, and Soil Science Society of America. All rights reserved. No part of this periodical may be reproduced or transmitted in any form or by any means, electronic or mechanical, including photocopying, recording, or any information storage and retrieval system, without permission in writing from the publisher.

Published in *J. Environ. Qual.* 37:XX-XX (2008).
 doi:10.2134/jeq2006.0281
 Received 19 July 2006.

*Corresponding Author (ThHarter@ucdavis.edu).

© ASA, CSSA, SSSA
 677 S. Segoe Rd., Madison, WI 53711 USA

T. Harter, Dep. of Land, Air, and Water, Univ. of California—Davis, Davis, California 95616-8628; E.R. Atwill, Veterinary Medicine Extension, School of Veterinary Medicine, Univ. of California—Davis, Davis, California 95616; L. Hou and B.M. Karle, Veterinary Medicine Teaching and Research Center, School of Veterinary Medicine, Univ. of California—Davis, Tulare, California 93274; K.W. Tate, Dep. of Plant Sciences, Univ. of California—Davis, Davis, California 95616.

Abbreviations: BTC, breakthrough curves; LME, linear mixed effect; SSDI, sterile degassed deionized.

Table 1. Soil physical properties measured from particle-size analysis (PSA) (Atwill et al., 2002) and estimated from the particle-size distribution using the NeuroMultistep transfer function (Minasny et al., 2004).

Soil	PSA Sand	PSA Silt	PSA Clay	NeuroMultistep θ_r	NeuroMultistep θ_s	NeuroMultistep α	NeuroMultistep n	NeuroMultistep K_p
	%			cm^{-1}				
Sandy loam	70	25	5	0.063	0.328	0.0069	2.63	5.3
Loam	45	37	18	0.107	0.402	0.0138	1.66	2.5
Clay	19	47	34	0.227	0.447	0.0113	1.53	0.52

settling, interception, and oocyst-surface interaction has provided an excellent tool to explain experimentally observed transport behavior of *C. parvum* oocysts (Brush et al., 1999; Harter et al., 2000; Marly et al., 2001). The fate of the 4- to 6- μm diameter oocysts is shown to be similar to that of other colloids of comparable geometry and surface properties. The framework also suggests that in fine-textured soils, oocyst transport in the soil matrix is extremely limited due to straining (Bradford et al., 2003; Bradford and Bettahar, 2005). Straining is the process of colloid immobilization between pore throats that are smaller than the colloid itself. Straining is the dominant removal process when the effective grain size diameter of the porous matrix is less than 20 times the size of the colloid (McDowell-Boyer et al., 1986). Given that the effective pore geometry in soils with nonuniform textural composition is determined by the finer grained elements, soils with more than 10% of clay or silt are not suitable for matrix transport of *Cryptosporidium* oocysts. The work by Bradford et al. (2003) suggests that straining may be a significant process for oocyst removal even in sand at grain size diameters exceeding 100 times the size of the colloid.

In a handful of *C. parvum* experiments that have been implemented with disturbed and undisturbed soils, significant and rapid transport of the oocysts through structured clay-loam, silt-loam, and loam soils was observed (Albrecht, 1996; Mawdsley et al., 1996a, 1996b; Atwill et al., 2002; Darnault et al., 2003, 2004). Similar observations have been made for the transport of other biocolloids and abiotic colloidal matter (e.g., McGechan and Lewis, 2002). In those cases, transport was attributed to flow in macropores due to soil structure, root canals, and biotic activity in the soils, but no further analysis of the flow processes was provided. In undisturbed soils with macropores and to a much lesser degree also in homogeneous sand columns, oocysts and other colloids have been observed to travel significantly faster than inert tracers due to size exclusion (e.g., Harter et al., 2000; Ginn et al., 2002; Poulsen et al., 2006).

This study examines the macropore-flow dominated transport dynamics of *C. parvum* in the shallow subsurface of vegetated, sloped soils during and after a rainstorm event. Our objectives were to estimate macropore properties relevant to *C. parvum* transport from precipitation data, static soil properties, and bromide breakthrough curves and to ascertain whether static soil properties and conservative tracer data are useful indicators to quantify the risk of *C. parvum* transport through shallow soils to such systems as tile drains; highly fractured bedrock; or shallow sandy, gravelly groundwater aquifers. We also tested some of our model assumptions by conducting a pair of saturated soil column studies to determine whether *C. parvum* transport was possible in the absence of macropores.

Materials and Methods

Soilbox Experiments

Details of the experimental design that generated the *C. parvum* transport data in shallow soils have been described previously (Atwill et al., 2002). Briefly, soilboxes were constructed of wood, sealed against leaks, and measured 15 cm wide \times 100 cm long \times 20 cm deep. Soils were air-dried, gently crushed, and passed through a 2-mm-pore-diameter sieve to remove coarse fragments. Soils were then dry-packed in 1- to 2-cm layers and hand-compacted before seeding. Perennial fescue seed was used to vegetate the soil. The grass cover was grown to >85% vegetative cover, using sprinkler irrigation, for at least 60 days before the experiment. Subsurface flow was captured through a slot at the bottom of the seepage face. Soils were selected to represent a wide range of soil textures present at animal husbandry locations in California (Table 1). The Hanford fine sandy loam, a Typic Xerorthent, was selected as a sandy soil with massive to weak fine granular structure and many very fine and fine interstitial pores. The Argonaut loam, a Mollic Haploxeralf, was selected as a loamy soil with weak fine subangular blocky structure and common very fine and fine but few medium pores. The Capay silty clay, a Typic Haploxerert, was selected as a clayey soil with moderate to very coarse prismatic structure and with common microtubular pores. All soils contained many very fine random roots due to the grass cover. Although roots were most dense in the upper 10 cm, many roots penetrated to a soil depth of 20 cm. Subsurface transport of *C. parvum* was evaluated for these three soils at three different slopes (5, 10, and 20%) for two simulated rainfall intensities (15 and 40 mm h^{-1} , referred to hereafter as "low" and "high" intensity, respectively), with three replicates per treatment, for a total of 54 trials. Mean vegetative cover (%) and mean vegetative height for each box were measured the day before the experiment. Two to four randomized boxes were irrigated simultaneously by a rainfall emitter, and a peristaltic pump delivered an oocyst suspension of 5×10^4 oocysts mL^{-1} for 60 min, initiating the start of the 4-h experiment. Each box received 10 mL min^{-1} from the pump, or 5×10^5 oocysts min^{-1} . After 60 min, the pump was switched back to water with no oocysts, and the simulated rain and peristaltic pump were continued for 180 min to quantify unbound or desorbed oocysts moving in the subsurface flow. The total number of oocysts that were collected in the outflow (surface runoff and subsurface outflow) ranged from 0.01 to 65% of the applied oocyst load. The median percentage of oocysts transported in the subsurface flow was 0.2% of the overland runoff.

Matrix Transport of Oocysts: Column Experiments

Samples of the three soils were sieved through a #35 mesh and dried at 70°C overnight. Dry soils were packed into Plexiglas col-

umns that were 5 cm in inner diameter and 10 cm in length. Both ends were covered by a layer of brass screen (#40 mesh or 380 μm) and a layer of stainless steel screen (0.5-mm holes). Both ends were sealed with a Plexiglas cap fitted with a flow port. Repacked bulk densities ranged from 1.5 g cm^{-3} for the fine-textured soils to 1.8 g cm^{-3} for the coarser-textured soil. Three columns, one of each soil type, were injected with CO_2 for 4 h at 6.89 kPa (1 psi). Next, 0.5 to 1 pore volume of sterile degassed deionized (SDDI) water with 50 mg L^{-1} of NaBr was injected using a peristaltic pump (Masterflex L/S; Cole and Palmer Instrument Company, Vernon Hills, IL), followed by 2 pore volumes of SDDI water and then 1 pore volume of SDDI water with 0.1 mM CaCl_2 . Next, we injected 1 pore volume of microbial stock solution (degassed deionized water containing 0.1 mM CaCl_2 , 10^6 oocysts mL^{-1} of *C. parvum*). The microbial stock solution was surrounded by an ice bath and kept in suspension on a stir plate during the hour-long injection. The soil columns were then injected with up to 13 pore volumes of SDDI water with 0.1 mM CaCl_2 to elute any unfiltered or detached oocysts. The microbial suspension was continually mixed on a stir plate during injection into the column. Flow rates were limited by the saturated hydraulic conductivity of the fine-textured soils and ranged from 1.5 to 5 cm d^{-1} . Column effluents for each soil series were continuously collected as 2-h composite samples using a fraction collector (CF-1 Fraction Collector; Spectrum Chromatography, Houston, TX) and held at 4°C until processed for protozoa enumeration.

Microbial Analysis

Details of the analytical procedures used to enumerate *C. parvum* in subsurface water samples have been described previously (Atwill et al., 2002). Briefly, naturally infected dairy calves from two local commercial dairies were the source of wild-type *C. parvum* oocysts. Oocysts were purified using discontinuous sucrose gradients, with the final oocyst concentration determined using a phase contrast hemacytometer. Quantitative immunofluorescent microscopy, using commercially prepared well slides (Meridian Diagnostics, Inc., Cincinnati, OH), and a fluorescein isothiocyanate-labeled anti-*Cryptosporidium* immunoglobulin M antibody (Waterborne, Inc., New Orleans, LA) were used to enumerate *C. parvum* oocysts. All enumerations were adjusted for the percent recovery of the assay (63–81% depending on soil type).

Modeling Analysis

The soils in the soilbox experiments are assumed to represent two coupled porous continua: a matrix pore space and a macropore space (dual porosity model). The matrix pore space represents the pores between tightly packed individual soil grains within soil aggregates. The macropore space is the interaggregate pore space created by soil maturation, shrinking and swelling, root growth and decay, and other biological activities in the root zone of the grass cover. Pore sizes associated with either pore space are highly variable, but the mean pore size of the macropore space is significantly higher than that of the matrix pore space (e.g., Beven and Germann, 1982). Some authors have suggested a continuum of pore sizes and divided the pore space into three domains specifically as a

function of pore size and associated capillary pressure (Shirmohammadi et al., 2005): micropores (conducting water flow below the field capacity of the soils), mesopores (conducting water flow when the moisture content exceeds field capacity), and macropores (conducting flow only when soil is near saturation).

Here, we do not distinguish between meso- and macroporosity. Furthermore, the matrix pore space and the macropore space are considered to be mutually continuous throughout the soilbox. Flow in both pore continua is considered to be Darcian. Transport in both pore continua is considered to be governed by an advection-dispersion-reaction type equation (see below). A numerical model of saturated matrix flow and transport in the soilbox experiments is constructed to compute the maximum possible contributions of the soil matrix (excluding the macropores) to total subsurface outflow and transport. Under saturated conditions, matrix flow rates are highest (relative to unsaturated flow). The model results are used to determine whether the observed 4-h breakthrough curves (BTCs) reflect matrix transport contributions or are solely due to macropore flow and transport. The dynamics of the measured breakthrough curves are used to infer the bulk hydraulic and transport characteristics of the macropore space (hydraulic conductivity, porosity, pathogen attenuation) through a simplified inverse solution of the dual porosity flow and transport equations. Although it is an approximation, this simplified, parsimonious model structure reflects the limited amount of hydraulic and transport property data available for these experiments.

Matrix Flow

To understand the processes affecting *C. parvum* transport, we determine the fractions of the subsurface outflow that can be attributed to macropore flow and to matrix flow. No direct measurements of either flow component or of the unsaturated hydraulic properties were performed during the experiment. Hence, the two flow components need to be estimated from corollary data, as is typically the case in field studies.

An upper limit for the amount of matrix flow in the uniformly packed soilboxes can be obtained by considering steady-state saturated flow under ponding conditions with homogeneous, isotropic hydraulic conductivity, K (cm d^{-1}). The flux vector, \mathbf{q} (cm d^{-1}), is obtained from Darcy's law:

$$\mathbf{q} = K\nabla b \quad [1]$$

where b (cm) is the pressure potential. Applying mass conservation, the distribution of the steady-state pressure potential is then governed by the Laplace equation:

$$\nabla^2 b = 0 \quad [2]$$

subject to the boundary conditions of the tilted soilbox experiment: At the surface of the soilboxes, shallow ponding is considered by setting a constant head boundary condition equal to the elevation of the surface of the soilbox. The subsurface outflow lip is also a constant head boundary condition with hydraulic head equal to its elevation. The remainder of the soilbox boundaries are no-flow boundaries. The solution to Eq. [2] and [1] is obtained by numerical

modeling using an implicit finite difference method (McDonald and Harbaugh, 1988).

Matrix Transport

Solute transport in the matrix is governed by the reactive advection-dispersion equation:

$$\frac{\partial c}{\partial t} = \theta D \frac{\partial^2 c}{\partial \mathbf{x}^2} - \frac{\partial \mathbf{q}c}{\partial \mathbf{x}} - \theta \lambda c \quad [3]$$

where t is time (d); \mathbf{x} is a three-dimensional position vector (cm); θ is the volumetric water content (-); D is the dispersion coefficient ($\text{cm}^2 \text{d}^{-1}$); and λ is a first-order attenuation factor (cm^{-1}) that accounts for degradation, deactivation, and filtration, as applicable (e.g., oocysts; Harter et al., 2000). Time and location dependency of the solute concentration, $c(x,t)$ (mg L^{-1}), is implied.

The matrix transport Eq. [3] is solved using a hybrid method of characteristics (Zheng and Wang, 1999). To imitate experimental conditions, a constant unit concentration of tracer is applied to the entire surface for the first 2 h of the experiment, followed by 2 h of clean infiltration. This condition is based on the observation of the bromide BTCs: Elevated concentrations (main breakthrough) were observed in the surface runoff for approximately 2 h (Atwill et al., 2002), although the injection at the top end of the soilbox ended after 1 h. Due to the location of the subsurface flow outlet, soil water and solute flux through the soilbox is highest near the surface runoff boundary at the downgradient end of the soilbox (see Results). Hence, we used the 2-h step-input function as a worst-case (conservative) approximation of solute flux into the surface of the soilbox.

Macropore Flow and Transport: Conceptual Model

The macropore flow domain is considered to be superimposed over the matrix flow domain (dual porosity media). The macropore flow domain consists of large interaggregate pores and root canals of unknown size and frequency, a situation commonly encountered in the analysis of field conditions. Under steady-state conditions and assuming relatively uniform macropore saturation throughout the soilbox, Eq. [1] and [2] provide a reasonable approximation of the flow field in the macropore domain, with the effective macropore hydraulic conductivity (K_o) replacing the matrix hydraulic conductivity (K) and the macropore flux (q_o) replacing the matrix flux (q) (Shirmohammadi et al., 2005). Transport in the macropore domain is governed by

$$\frac{\partial c_o}{\partial t} = \theta_o D_o \frac{\partial^2 c_o}{\partial \mathbf{x}^2} - \frac{\partial \mathbf{q}_o c_o}{\partial \mathbf{x}} - \theta_o \lambda_o c_o \quad [4]$$

where the subscript o indicates transport properties specific to the macropore domain. The pressure distributions between the matrix- and macropore domains are coupled. Hence, under steady-state conditions, the pressure head profiles in the macropore domain and in the matrix domain are approximately identical. We therefore assume that the advective water flux exchange between the two domains is negligible and that the normalized flux field is identical for both domains, $q_o K_o^{-1} = q K^{-1}$. Solute transport in

the two domains is coupled through diffusive exchange of solutes. However, during the 4-h experiment, macropore fluxes dominate the transport (see below), and the contribution of diffusive fluxes between the two domains is considered to be negligible. Therefore, diffusive exchange need therefore not be included in Eq. [4].

The parameters controlling nonreactive and reactive transport in the macropore domain are the macropore water content (θ_o) and the macropore flow rate (q_o), which in turn are controlled by K_o . The filtration of the oocyst in the macropore space is controlled through the filtration rate (λ_o).

Macropore Flow and Transport: Parameter Estimation

Here, we use the experimental data collected at the surface and subsurface outlets of each tilted soilbox to estimate q_o , K_o , θ_o , and net oocyst attenuation over the 20-cm depth through a simple inverse solution of Eq. [2] and [4]. Let us denote the observed peak bromide and *C. parvum* concentration in the surface outflow BTC as c_{Br-in} and c_{Cp-in} and the peak bromide and *C. parvum* concentration in the subsurface outflow BTC as c_{Br-out} and c_{Cp-out} . The difference in arrival time between the peak concentration in the soil surface BTC and the peak concentration in the subsurface BTC is denoted Δt_{Br} and Δt_{Cp} for bromide and *C. parvum*, respectively.

Owing to the sustained input of bromide at the soil surface over a 2-h period, the peak concentration of bromide transported through the macropore domain is not significantly affected (reduced) by diffusion into the matrix domain or by hydrodynamic dispersion. Hence, the subsurface outflow peak bromide concentration is a mixed aqueous solution of macropore outflow with macropore concentration $c_o - c_{Br-in}$ and matrix outflow with matrix concentration $c - 0$ before $t = 3$ h (see flow modeling results below):

$$(q_o + q)c_{BR-out} = q_o c_{BR-in} + q \times 0 \quad [5]$$

The sum ($q_o + q$) is the total subsurface outflow rate, which has been measured. The q_o can, therefore, be obtained by solving Eq. [5]:

$$q_o = (q_o + q) \frac{c_{BR-out}}{c_{BR-in}} \quad [6]$$

Assuming relatively uniform moisture distribution, the average θ_o can be determined from the ratio of the macropore flux rate and the average linear macropore velocity (v_o):

$$\theta_o = \frac{q_o}{A_{out} v_o} \quad [7]$$

where A_{out} is the surface area (cm^2) of the subsurface outflow interface. A lower-bound estimate of the average v_o (cm d^{-1}) in the macropore domain is obtained by considering that the bulk of the bromide transport occurs from the soilbox surface directly above the subsurface outflow lip to the lip itself, a distance of slightly more than 20 cm (see flow modeling results below). Dividing that distance by the travel time for the peak concentration (Δt_{Br}) we obtain an approximation of v_o .

The macropore (unsaturated) effective hydraulic conductivi-

ty can be obtained from q_o and the flow solution of the numerical model of Eq. [2]: If q' is the reference outflow rate obtained for $K' = 1 \text{ cm d}^{-1}$ (different at different soil slopes), then

$$K_o = K' \frac{q_o}{q'} \quad [8]$$

The filtration factor in Eq. [4], λ_o , depends on the local pore velocity and generally varies throughout the soilbox due to the non-uniform pore velocity conditions, which increase substantially in the immediate vicinity of the subsurface outflow lip. Noting that the area contributing most to solute transport is the vertical flow field region near the lower end of the soilbox, we assume a quasi-one-dimensional solution with a constant effective filtration factor, $\Lambda_{\text{eff}20}$ (dimensionless), that is representative for the total filtration in the 20-cm thick soil. Hence, the total reduction of *C. parvum* oocyst concentration due to filtration can be approximated by:

$$\frac{c_{\text{Cp-out}}}{c_{\text{Cp-in}}} = \frac{q_o}{q_o + q} \exp(-\Lambda_{\text{eff}20}) \quad [9]$$

where the first term on the right-hand side reflects the dilution due to mixing of matrix and macropore outflow in the captured subsurface outflow sample. Using Eq. [6], we obtain from Eq. [9] after rearranging:

$$\Lambda_{\text{eff}20} = \ln \left(\frac{\frac{c_{\text{Br-out}}}{c_{\text{Br-in}}}}{\frac{c_{\text{Cp-out}}}{c_{\text{Cp-in}}}} \right) \quad [10]$$

Statistical Analyses

A linear mixed effect (LME) model (Pinheiro and Bates, 2000) was used to quantify the association between the estimated effective macroporosity characteristics (dependent variables) and the experimental covariates or independent variables (soil type, bulk density, slope, rainfall intensity, and grass maturity). Linear mixed-effects regression was chosen as the statistical model due to the fact that our data structure included fixed effects (the experimental covariates) and a group or random effect (irrigation trial) in which two to four soilboxes were irrigated simultaneously by a rainfall emitter to generate the overland- and subsurface flow conditions (Atwill et al., 2002). Due to subtle experimental differences between each irrigation trial, the dependent data generated from each trial of two to four boxes was slightly correlated within trial, requiring that the statistical model properly adjust the fixed-effect coefficients and their estimated variances for this lack of independence (Pinheiro and Bates, 2000). The resulting statistical models provide predictive tools for site-specific macropore flow and *C. parvum* transport properties. We used a forward stepping algorithm to build the model, with significance for inclusion of the experimental covariates in the regression model set at $P \leq 0.10$.

Logistic regression (Agresti, 2002; Haan, 2002) was used to calculate the probability of observing *C. parvum* in macropore flow as a function of subsurface flow, soil static properties, and the rate of precipitation. We used a forward stepping

algorithm to build the model, with significance for inclusion of the experimental covariates in the model set at $P \leq 0.10$.

Results and Discussion

Matrix Flow and Transport in the Tilted Soilboxes:

Theoretical Limits

Theoretical pressure head solutions of Eq. [2] subject to the tilted soilbox boundary conditions are shown in Fig. 1 for the 5 and 20% slope. Also shown is the normalized flux field, $q K^{-1}$, obtained from Eq. [1] (indicated as arrows). Neither the pressure head, h , nor $q K^{-1}$ depend on the actual magnitude of K . The cross-section indicates that the majority of the subsurface outflow is generated by water infiltrating near the lower end of the tilted soilboxes. The fastest and most significant flow path is an approximately straight vertical path from the soilbox surface to the subsurface outlet. Due to the continuity in the hydraulic pressure distribution, the macropore flow field is thought to effectively follow the same pattern as the computed matrix flow field.

From the model, a normalized outflow rate q' for a unit hydraulic conductivity (1 cm d^{-1}) is obtained after integrating across the outflow interface ($q' = 31, 32, \text{ and } 34 \text{ mL in } 4 \text{ h}$ for slopes of 5, 10, and 20%, respectively). The slope of the tilted soilboxes is found to have little effect on the subsurface flow rate. This is consistent with the observation that almost all simulated flow occurs near the lower end of the box, where the flow distance through the soil and the hydraulic gradient are nearly unchanged at different slopes. Estimated saturated matrix flow rates are obtained by multiplying q' with the hydraulic conductivity for the specific soil (in cm d^{-1}) because the outflow rate scales linearly with the hydraulic conductivity (Eq. [1]). The specific soil hydraulic conductivities were estimated using a soil texture-based transfer function approach (Minasny et al., 2004). The mean estimates of K are 0.5, 2.5, and 5 cm d^{-1} for the clay silt loam, loam, and sandy loam, respectively (Table 1). The estimation is approximate and has a significant margin of error (\pm half an order of magnitude, higher for the clay silt loam). Hence, the maximum expected subsurface outflow contribution from matrix flow in the soilbox over the 4-h sampling period ranges from approximately 15 mL (5–50 mL) in the 5% slope Capay silty clay loam soilboxes to approximately 170 mL (50–500 mL) in the 20% slope Hanford sandy loam soilboxes.

Theoretical concentration profiles at the end of the 4-h experiment and the hypothetical subsurface outlet BTCs are also shown in Fig. 1 for three different values of K . These BTCs, representing bromide transport in the matrix domain, were computed by solving Eq. [4] for the two-dimensional, saturated matrix flow system (Fig. 1) with $\lambda = 0$ (nonreactive transport). The bromide that first arrives at the subsurface outlet originates from the soilbox surface directly above the subsurface outflow lip just upstream of the surface outflow lip.

In our experiments, the maximum hydraulic conductivity (in the range of $2\text{--}20 \text{ cm d}^{-1}$) is associated with the sandy loam. The theoretical computations show that even for high K values, bromide breakthrough from matrix transport is insignificant until very late in the 4-h experiment. Consequently, any bromide breakthrough before $t = 3 \text{ h}$ must be attributed to macropore transport.

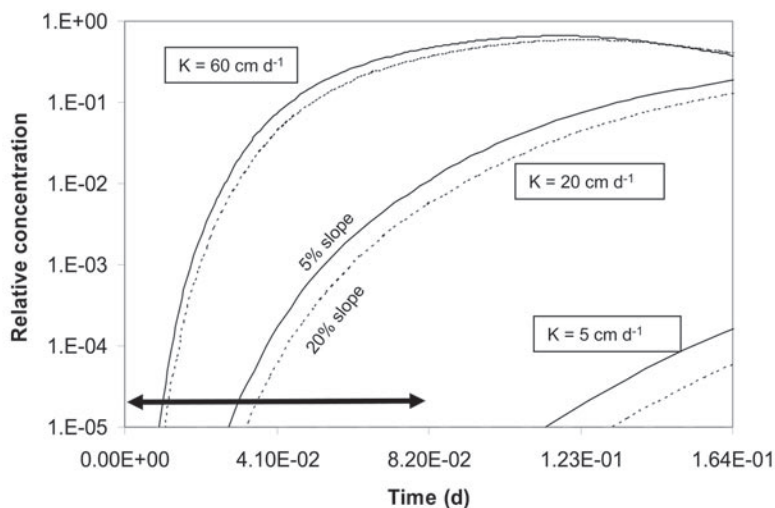
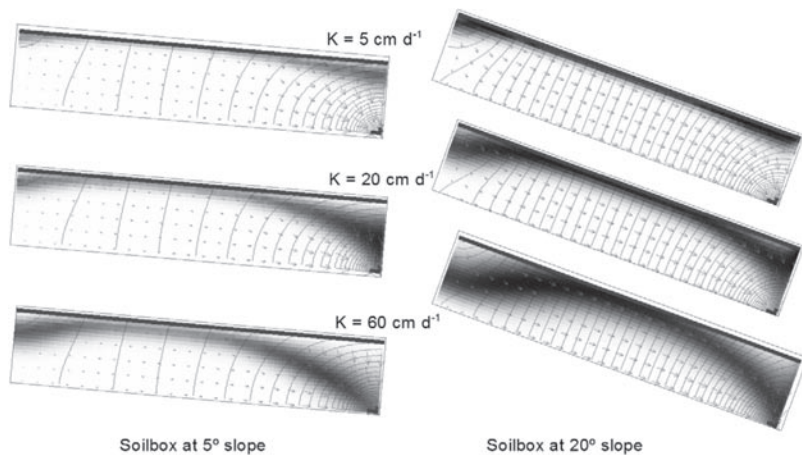


Fig. 1. Results from the numerical modeling analysis of matrix flow and transport in the soilbox experiments: Distribution of equipotential lines, velocity field, and tracer concentration (gray-scale) for three different hydraulic conductivities at 5% slope (top left) and 20% slope (top right). Resulting breakthrough curves at the lower right hand outflow lip over a 4-h period (bottom). Due to the steady-state conditions, the equipotential lines are assumed identical for the matrix and macropore domain. Hence, the orientation of the velocity field is representative of both domains.

Cryptosporidium parvum during transport in porous media is subject to sorption–desorption, filtration and straining (Brush et al., 1999; Harter et al., 2000; Bradford and Betahar, 2005). Straining (i.e., removal of the oocyst due to trapping in pore-throats that are smaller than the diameter of the oocyst) is the most significant removal mechanism in porous media with an effective grain size less than approximately 100 μm to 1 mm (20–200 \times the oocyst diameter) (McDowell-Boyer et al., 1986; Bradford et al., 2003). The latter condition dominates all three soils tested: although highly non-uniform, d_{10} values for clay and loam are less than 2 μm and for the sandy loam are between 2 and 50 μm , well below the straining threshold. The 10th percentile passing grade, d_{10} , is the particle size representing the smallest 10th percentile in the grain size distribution and is used as a measure for the effective grain size with respect to colloid transport. Therefore, *C. parvum* is not expected to be transported through the matrix of the packed soilboxes.

Two replicate column experiments were conducted to ascertain that no *C. parvum* transport occurred through the soil matrix, with each experiment examining the ability of the three different soil types to completely retain *C. parvum* under saturated, matrix flow conditions (i.e., no macropores present; flow limited to micropore spaces between soil grains). None of the effluent water samples tested from either of the columns from each of the three soils had detectable levels of *C. parvum* oocysts, indicating that this protozoal parasite was removed during subsurface transport under matrix flow conditions. Hence, the observed *C. parvum* transport must be attributed to macropore flow.

Observed Subsurface Flow and Transport

The total amount of observed subsurface outflow over the 4-h soilbox experiment, Q_{tot} , varied from less than 10 to over 10,000 mL. The geometric mean outflow rate was 672 mL for the entire dataset, 249 mL for the low-intensity rainstorm (Rainstorm 1), and 1954 mL for the high-intensity rainstorm (Rainstorm 2). The median percentage of total effluent collected from subsurface outflow was 4%. The subsurface outflow is highly variable and log-normally distributed (Fig. 2). The amount of subsurface outflow in many experiments is significantly larger than the highest estimated matrix outflow rate for even the coarsest soil (50–500 mL per 4 h), which is further indication that macropore flow constitutes a significant fraction of the subsurface outflow in many of the experiments. The significant difference in subsurface outflow between the two rainfall events also suggests that the soilboxes were not completely saturated, at least not under low-intensity rainfall conditions. Increasing saturation of the macropore domain under the higher rainfall rate allowed for a significant increase in infiltration and subsurface outflow. At least for the low intensity rainfall, the matrix flow rate is, therefore, thought to be much lower than the saturated-flow-based upper-bounds stated previously. These findings substantiate the significant role of macropore flow in the experiments and provide justification for the use of the inverse modeling procedure described here to estimate macropore properties from the subsurface outflow and transport data.

Similar to subsurface outflow, the observed BTCs of bromide and *C. parvum* varied widely in their characteristics. Given the bounds determined from the matrix flow and transport modeling, we grouped the individual BTCs into two categories: bromide BTCs that indicated significant macropore flow (i.e., with a BTC that had a clear increase, saddle, and decrease in concentration before the completion of the 4-h experiment [BrBTC = 1]) and bromide BTCs that did not indicate macropore flow (i.e., those with no or relatively small amounts of bromide or those with bromide concentrations increasing only very late in the experiment [after $t = 3$ h, BrBTC = 0]). Similarly, *C. parvum* BTCs

were grouped into BTCs that had a distinct saddle or at least a continuous, if only relatively flat, breakthrough of *C. parvum* ($C_p\text{BTC} = 1$) and experiments with no confirmed detections of *C. parvum* ($C_p\text{BTC} = 0$). “Confirmed detections” are defined as BTCs with at least three detections at levels significantly above the detection limit. Average bromide and *C. parvum* BTCs for each of the two indicator classes are shown in Fig. 3. The mean oocyst concentration for $C_p\text{BTC} = 0$ is computed from very few values of BTCs, with at most two detections at random times. For comparison, average surface runoff BTCs, which represent the source term for subsurface transport (see Fig. 1), are shown. As expected, concentrations of bromide and *C. parvum* for $\text{BrBTC} = 0$ and $C_p\text{BTC} = 0$ do not show a breakthrough (random low values). For $\text{BrBTC} = 1$ and $C_p\text{BTC} = 1$, the average BTCs have a significant attenuation in peak concentration relative to the BTC at the surface of the box, but there is no significant delay in the location of the peak time between the surface and subsurface BTCs, indicating relatively fast transport through the soil macropore space. The total number of oocysts captured from subsurface outflow represents a median of 0.2% of the total oocysts collected in surface outflow. Overall, the total number of oocysts collected in surface and subsurface outflow ranged from 0.01 to 65% of the initial oocyst load (Atwill et al., 2002).

Estimated (Fitted) Parameters of Macropore Flow and Transport

Using the bromide data as input to the simplified inverse solution of the dual domain flow system, bulk hydraulic properties of the soilbox macropore domain (K_o , θ_o , v_o) were obtained for each experiment that exhibited significant early bromide breakthrough ($\text{BrBTC} = 1$). Net oocyst attenuation ($\Lambda_{\text{eff}20}$) obtained from the *C. parvum* data was computed for those experiments that also had *C. parvum* breakthrough ($\text{BrBTC} = 1$ and $C_p\text{BTC} = 1$).

Estimated values of θ_o , K_o , and $\Lambda_{\text{eff}20}$ of *C. parvum* vary significantly among the individual experiments (Table 2). Water content and hydraulic conductivity of the macropore domain are approximately lognormally distributed. Macropore water content values obtained from *C. parvum* data ($C_p\text{BTC} = 1$) are slightly higher than, but strongly correlated to, those obtained from bromide data ($\log_{10} \theta_o^{\text{Cp}} = 0.067 + 0.88 \log_{10} \theta_o^{\text{Br}}$; $r^2 = 0.80$). In contrast, the linear pore velocities, v_o , obtained from the oocyst and bromide breakthrough (both based on first significant arrival) are uncorrelated. Linear pore velocities larger than 20 cm per 10 min = 2 cm min⁻¹ could not be measured (20 cm: shortest possible subsurface travel path; 10 min: sample collection interval). In most experiments, velocities are estimated to fall within the three fastest measuring bins: 0.67, 1, or 2 cm min⁻¹. The lack of resolution at an early time may explain the lack of correlation between pore velocities estimated for *C. parvum* and those estimated for bromide.

The simple inverse model to derive macropore properties does not always yield physically reasonable results. In 5 of 42 experiments, the observed linear pore velocity (obtained from the travel time of bromide) was on the same order or smaller than the observed q_o , leading to unreasonably large water content estimates for the macropore domain. In 6 out of 34 experi-

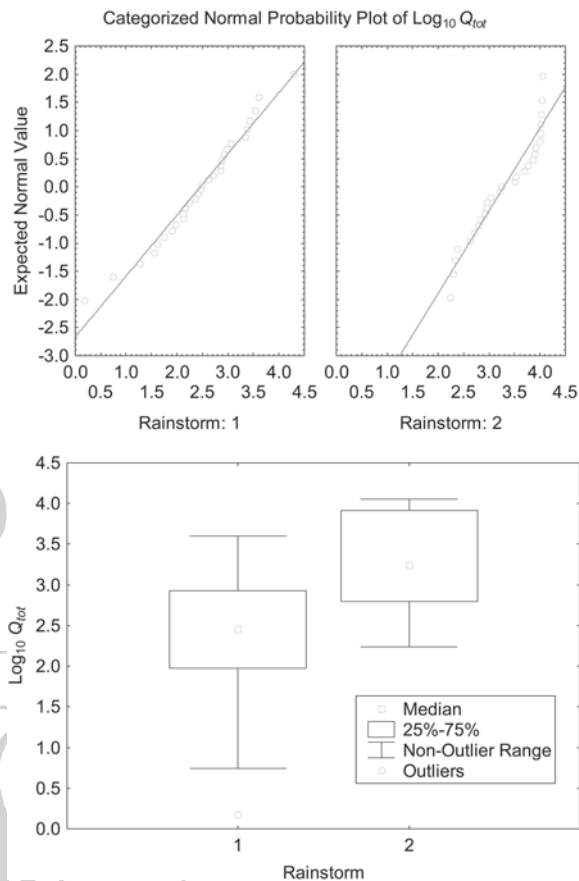


Fig. 2. Normal probability plot (top) and quantiles (bottom) of measured subsurface outflow rates for each of the two rainstorms (15 and 40 mm h⁻¹, respectively). Q_{tot} : total outflow volume (mL).

ments, *C. parvum* concentrations in the subsurface outflow were less diluted (relative to surface runoff concentrations) than bromide, leading to negative attenuation factors. In those cases, distinct heterogeneous patterns in the hydraulic field of the soilboxes may have dominated and are not accounted for by the simple conceptual-mathematical model used here.

Predicting Macropore Flow and Transport Parameters from Site Conditions: LME Modeling

The LME modeling was used to determine the amount of variability in K_o , θ_o , and v_o that can be statistically explained by soil type, slope, grass height, bulk density, and rainfall intensity. Soil type, slope, and grass height are readily measurable site properties, often available from maps or field measurement. Rainfall intensity controls the amount of water available for infiltration and, hence, the saturation of the soil matrix and macropore domain. Bulk density is a readily measured soil property in watershed studies and has been shown to be directly related to macroporosity (e.g., Messing et al., 1997; Mori et al., 1999a,b). For the LME modeling, we included only those experiments with physically plausible parameter estimates (i.e., with $0 < \theta_o < 1$ and with $\Lambda_{\text{eff}20} \geq 0$).

A significant association was found between macropore properties (K_o , θ_o) and bulk density and rainfall intensity (Table 3). For example, for each 0.1 g cm⁻³ increase in bulk density, the

effective θ_0 decreases by a factor of 0.75 ($10^{-1.256 \times 0.1} = 0.75$). At the high rainfall rate, θ_0 is about 3.7 times larger ($10^{0.574} = 3.7$) compared with θ_0 at the lower rainfall rate. At the lower rainfall rate, significant moisture (>2% by volume, $\theta_0 > 0.02$) is found in the macropore space only at bulk densities of 1.3 g cm^{-3} or less,

whereas the high rainfall rate creates significant macropore moisture at much higher bulk densities (1.7 g cm^{-3} or less), according to this model (Fig. 4a). Similarly, for each 0.1 g cm^{-3} increase in bulk density, the K_0 decreases by a factor of 0.81 ($10^{-0.899 \times 0.1} = 0.81$). At the higher rainfall rate, the K_0 is about 6.5 times larger ($10^{0.816} = 6.5$) compared with K_0 at the lower rainfall rate (Fig. 4b).

The significantly higher θ_0 at the higher rainfall rate is thought to be due to increased saturation of the macropore domain and due to a significant increase in the number of macropores participating in subsurface flow at the higher rainfall rate (Shirmohammadi et al., 2005). The increase in macropore hydraulic conductivity at the high rainfall rate is consistent with our conceptual understanding of unsaturated hydraulic conductivity (Shirmohammadi et al., 2005; Hillel, 2004).

Slope did not significantly affect the effective macropore domain properties, which is consistent with the findings from the numerical model (Fig. 1). Soil type also did not serve as a significant indicator of macropore domain properties. We found no significant associations between the linear pore velocity estimates (v_0), and abiotic factors in the experiment, possibly due to poor resolution of pore velocity measurements.

Bulk density is a proxy measure of total available macropore space (θ_0 at saturation), whereas the estimated θ_0 represents only the amount of active macropore space (macropore space participating in flow): As bulk density increases, the maximum macropore space available for flow and transport decreases. Bulk density in the ensemble of the tilted soilboxes is significantly associated with soil type and root growth as expressed by grass height (Table 4), although a direct association between $\log K_0$ (or $\log \theta_0$) and soil type or grass height was not found using LME. Bulk density is predicted to be highest in the sandy loam (less macropore space and smaller macropore size) and lowest in the clay (more macropore space

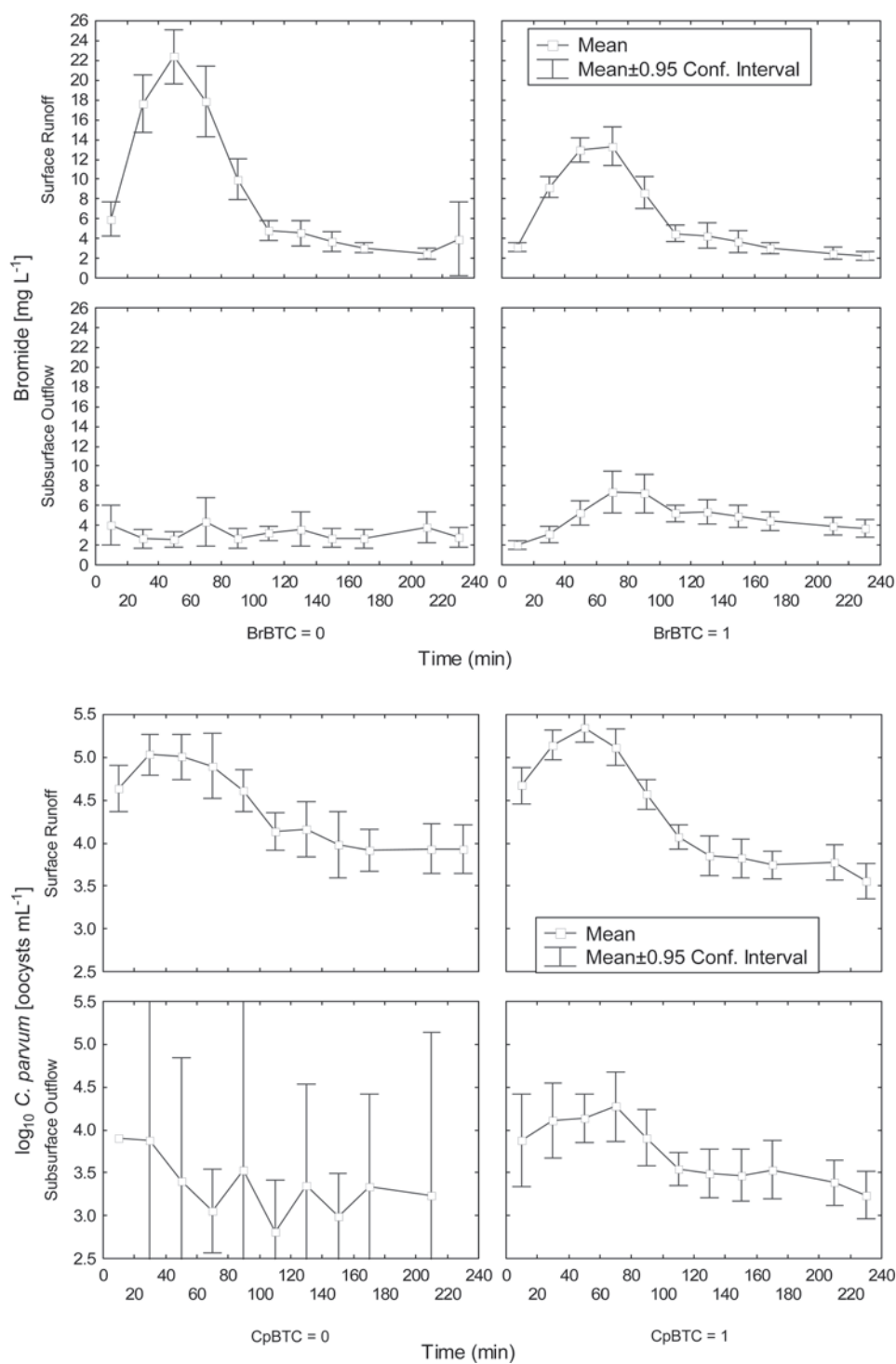


Fig. 3. Bromide breakthrough curves (BrBTC) (top panel) and *Cryptosporidium* BTC (CpBTC) (bottom panel) in surface runoff (first row of each of the two panels) and in subsurface outflow (second row of each of the two panels). Left: Mean, minimum, maximum, and 95% confidence interval of the mean concentration for experiments with BrBTC = 0 (bromide BTCs) or CpBTC = 0. Right: As on the left side, but for BrBTC = 1 and CpBTC = 1, respectively.

Table 2. Descriptive statistics of those parameters that were determined from the simplified inverse solution to dual porosity flow.

	Valid N	Mean	Median	Minimum	Maximum	Lower quartile	Upper quartile	Variance	SD	SE
BrBTC = 1										
V_o^{BR}	42	1.617	1.000	0.143	4.000	0.500	2.000	1.917	1.385	0.214
$\log_{10} TH_o^{BR}$	42	-1.196	-1.252	-2.907	0.631	-2.072	-0.412	0.855	0.924	0.143
$\log_{10} K_o^{BR}$	42	1.150	1.107	-0.522	2.514	0.373	1.906	0.802	0.896	0.138
CpBTC = 1										
Λ_{eff20}	34	0.578	0.720	-1.869	1.888	0.228	0.939	0.520	0.721	0.124
V_o^{CP}	36	0.883	0.667	0.222	2.000	0.667	1.333	0.189	0.435	0.072
$\log_{10} TH_o^{CP}$	36	-1.089	-1.055	-3.505	0.330	-1.704	-0.283	0.990	0.995	0.166

† BrBTC: bromide breakthrough curve quality (exists: 1; no breakthrough: 0); CpBTC: C. parvum breakthrough curve quality (exists: 1; no breakthrough: 0); V_o^{BR} : macropore velocity (cm min⁻¹) obtained from the bromide BTC; $\log_{10} \theta_o^{BR}$: macropore water content (cm³ cm⁻³) obtained from the bromide BTC; $\log_{10} K_o^{BR}$: macropore hydraulic conductivity (cm d⁻¹) obtained from the bromide BTC; Λ_{eff20} : attenuation coefficient (dimensionless) for oocyst transport (filtration factor); V_o^{CP} : macropore velocity (cm min⁻¹) obtained from the oocyst BTC; $\log_{10} \theta_o^{CP}$: macropore water content (cm³ cm⁻³) obtained from the oocyst BTC.

and larger macropore size due to stronger shrinking-swelling). Increasing grass height and associated root growth also results in lower bulk density (more macropore space). Grass height is directly related to root density (Kirkham, 2005), which in turn affects total macropore space.

The Λ_{eff20} varies from just above 0 to nearly 2, with an average attenuation of 0.6. In other words, the 20-cm-thick soil achieves an average attenuation of slightly more than half an order of magnitude. The Λ_{eff20} was found to be associated with macropore properties obtained from the C. parvum BTCs $\log_{10} \theta_o^{CP}$ and $\log_{10} K_o^{CP}$ (only experiments with CpBTC = 1; Table 5 and Fig. 5). The attenuation decreases by 1.03 for each order of magnitude increase in effective unsaturated K_o and increases by 1.13 for each order of magnitude increase in effective θ_o .

The model suggests that higher θ_o yields larger effective attenuation. This is consistent with the alternative LME model association between attenuation, bulk density, and rainfall intensity (Table 3). For example, for each 0.1 g cm⁻³ decrease in bulk density (and by corollary an increase in total macropore content), there is an associated increase in Λ_{eff20} by 0.027 at low rainfall intensity but a much higher increase of 0.14 at high rainfall intensity. At high bulk densities (1.5–1.7 g cm⁻³), the attenuation rate is similar between the two rainfall intensities. For bulk densities of 1.5 g cm⁻³ or less, the attenuation is significantly higher at the high rainfall intensity than

at the low rainfall intensity (Fig. 4e). This pattern is consistent with the findings of Atwill et al. (2002) who showed that, given a specific subsurface outflow rate, the total amount of nonfiltered oocysts was higher at the low rainfall intensity.

The decrease in attenuation with increasing bulk density and less attenuation at lower rainfall intensity at lower bulk density is surprising at first glance: Higher bulk density is synonymous with less macropore volume and lower θ_o . Common intuition may sug-

Table 3. Final linear mixed effects regression models† for abiotic factors associated with macropore hydraulic conductivity (cm d⁻¹), macropore water content (cm³ cm⁻³), and C. parvum effective attenuation rate (dimensionless). The maximum absolute standardized within-group residuals for these three models are 1.83, 2.05, and 2.87, respectively (see Fig. 4).

Abiotic factors	Mean{log K_o }‡ (SD)	Regression coefficient for Log{macropore hydraulic conductivity}‡ (SE)	P value§
Rain storm			
Low intensity¶	0.65 (0.79)	0.0 (-)	-
High intensity	1.33 (0.77)	0.816 (0.294)	0.017
Bulk density (BD)#	1.00 (0.84)	-0.899 (0.482)	0.076
Intercept	-	1.733 (0.606)	0.009
	Mean{log θ_o }‡ (SD)	Regression coefficient for Log{macropore water content}‡ (SE)	P value§
Rain storm			
Low intensity¶	-1.59 (0.80)	0.0 (-)	-
High intensity	-1.20 (0.78)	0.574 (0.304)	0.084
BD#	-1.39 (0.80)	-1.256 (0.454)	0.011
Intercept	-	-0.075 (0.577)	0.90
	Mean{ Λ_{eff20} }‡ (SD)	Regression coefficient for effective attenuation rate‡ (SE)	P value§
Rainstorm			
Low intensity¶	0.72 (0.27)	0.0 (-)	-
High intensity	0.87 (0.47)	1.743 (0.766)	0.046
BD#	0.81 (0.40)	-0.267 (0.376)	0.49
Rainfall × BD interaction			
low intensity×BD¶	-	0.0 (-)	-
high intensity×BD	-	-1.106 (0.571)	0.082
Intercept	-	1.040 (0.470)	0.051

† Abiotic factors (e.g., soil series, slope, rainfall, bulk density) were modeled as fixed-effects; experiment (15 randomized sets of two to four soilboxes per experiment) was modeled as a random effect; outcome variable was the decadal logarithm of the macropore hydraulic conductivity (K_o), the decadal logarithm of macropore water content (θ_o), and the effective attenuation rate (Λ_{eff20}).

‡ As estimated from the inverse model. To obtain the regression coefficients for log K_o and for log θ_o we considered only experiments for which $\log_{10} \theta_o < 0$ and for which the bromide breakthrough curve (BTC) existed (37 experiments). To obtain the regression coefficients for Λ_{eff20} we considered only experiments for which $\log_{10} \theta_o^{CP} < 0$, for which the oocyst BTC existed, and for which Λ_{eff20} not less than zero (24 experiments).

§ P value determined from conditional t test.

¶ Referent category.

Bulk density: g cm⁻³ of oven-dried soil.

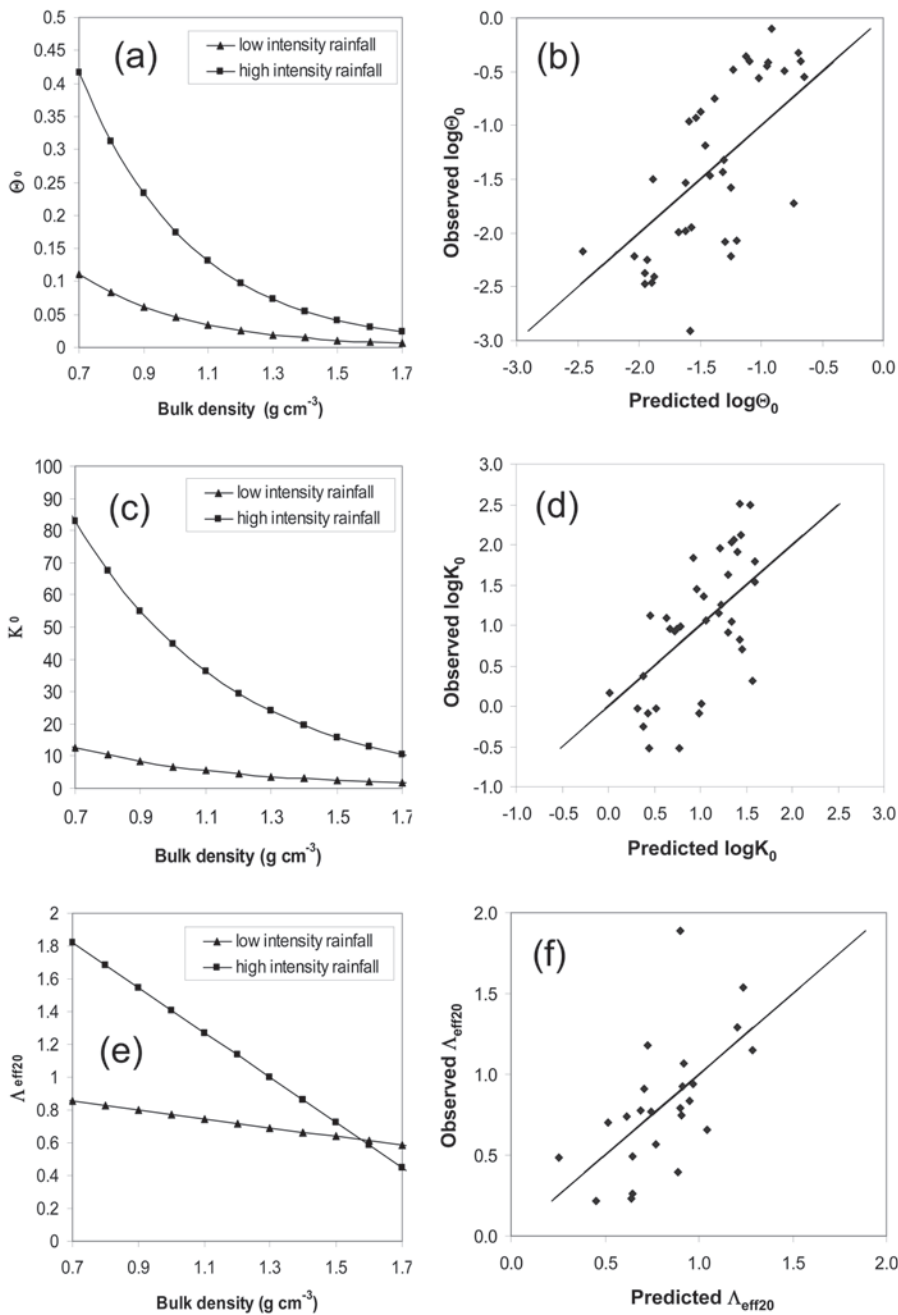


Fig. 4. Linear mixed effects (LME) model predictions (left side) for (a) macropore water content, θ_0 ($\text{cm}^3 \text{cm}^{-3}$), (c) macropore hydraulic conductivity, K_0 (cm d^{-1}), and (e) oocyst attenuation, $\Lambda_{\text{eff}20}$ (dimensionless), as a function of bulk density. The LME model predicted values are compared with measured (observed) values (right side). Comparing observed and predicted values of the three variables, the SEs are 0.67, 0.59, and 0.34, respectively. Further statistical evaluation of the LME model is given in Table 3.

gest higher attenuation in the smaller pore space (i.e., larger oocyst attenuation at higher bulk density). Lower rainfall rates mean less subsurface flow, suggesting more attenuation.

Physico-chemical processes may also explain the observed opposite effect: First, the higher pH (6.7) of the sandy loam soil, which exhibited the highest bulk density, is less favorable for oocyst attachment than the lower pH of the other two finer-textured soils with the lower bulk density (6.0 and 5.5). The reason is that the zeta-potential of the oocysts is more negative at higher pH, lead-

ing to less attachment onto soil particles (Searcy et al., 2005). Second, and more importantly, it has been shown that oocysts become attached to the air–water interface when pores are unsaturated, thus increasing significantly the retention and retardation of the oocysts (Darnault et al., 2004; Zevi et al., 2005). The overall macropore size in the sandy loam soil is likely smaller than in the shrink-swell affected loam and clay-loam soils. Under variably saturated conditions, the smaller macropores of the sandy loam soil may become saturated at significantly lower water content, providing less air–water interface area for attenuation than the larger macropores of the finer-textured, structured soils. The latter remain unsaturated with significant air-pockets within the macropore system. Third, at the higher rainfall intensity, increased swelling of the structured clayey soils may contribute to a significant decrease in the available pore space, thus effectively increasing the attenuation in the lower bulk density soils.

The LME analysis suggests that although the macropores are larger and θ_0 is higher in the finer-textured soils with lower bulk density, oocysts are more efficiently transported in the narrower, less abundant, non-swelling, and more saturated macropores (defined as “mesopores” by Shirmohammadi et al., 2005) of the less acidic and denser sandy loam soils, at least under our experimental conditions. Consistent with this hypothesis, we find a weak positive correlation between the travel time of the oocysts and the amount of oocyst attenuation. It seems that the linear pore velocities in the macropore space are greatly accelerated at the higher bulk density (lower θ_0 , narrower macropores), leading to the rapid transport of the oocysts through the soilbox. Further research is needed to rigorously test these hypotheses.

In summary, the overall consistency of these statistical models with fundamental principles of soil physics and the consistency of the estimated magnitudes in unsaturated θ_0 and hydraulic conductivity with field measurements demonstrate that the simple inverse modeling approach applied here provides useful estimates of the upscaled, effective flow and transport properties of the macropore space. Furthermore, these LME models suggest that the amount of *C. parvum* attenuation in the tested agricultural soils is highly dependent on the distribution of macropore structures and their level of saturation.

Table 4. Final linear mixed-effects regression model† for soil series and grass height associated with bulk density.

Fixed effects	Mean bulk density‡ (SD)	Regression coefficient for bulk density‡ (SE)	P value§
Soil series			
Silty clay loam§	1.06 (0.23)	0.0 (-)	-
Loam	1.25 (0.20)	0.144 (0.043)	0.0018
Sandy loam	1.49 (0.16)	0.444 (0.040)	<0.0001
Grass height (cm)	1.27 (0.27)	-0.010 (0.003)	0.0037
Intercept	-	1.279 (0.091)	<0.0001

† Grass height and soil type were modeled as fixed-effects; experiment (15 randomized sets of two to four soilboxes per experiment) was modeled as a random effect; outcome variable was bulk density.

‡ Bulk density (g cm^{-3}) obtained from measurements at each of 56 experiments.

§ P value determined from a conditional t test.

Predicting the Risk of *C. parvum* Transport from Flow and Tracer Observations

Vegetated buffers are widely advocated as a practical and effective means to reduce the transport of *C. parvum* from terrestrial to aquatic systems. Implicit in this recommendation is that waterborne *C. parvum* oocysts that infiltrate into the soil profile are filtered or otherwise retained before entering shallow groundwater, tile drains, or some form of return flow. Substantial amounts of *C. parvum* breakthrough in subsurface flow via macropores suggests that shallow groundwater and surface water under the influence of return flow are at risk of *C. parvum* contamination (Svoboda et al., 1999; De Carvalho et al., 2000; Moulton-Hancock et al., 2000; Morris and Foster, 2000; Bicudo and Goyal, 2003). This motivated us to determine if there are practicable measurements other than direct oocyst analysis that may be useful predictors of significant *C. parvum* transport through the soil zone.

The dataset generated from the box experiments yielded two indicators associated with the relative magnitude of macropore flow: the macropore flux ratio (Q_r'), defined as the ratio of the total subsurface flow rate to the estimated mean matrix flow rate (at $K = 0.5, 2.5,$ and 5 m d^{-1} for the three soils, respectively) and the occurrence of significant early bromide breakthrough in subsurface flow (BrBTC = 1). Because the occurrence of *C. parvum* in the subsurface is intrinsically linked to the occurrence of macropore flow, we questioned whether these two indicators are capable of predicting the probability of significant *C. parvum* transport through the soil zone.

Significant *C. parvum* breakthrough (CpBTC = 1) was observed in 37 of 56 experiments, and early bromide breakthrough (BrBTC = 1) was observed in 42 of 56 experiments. In nine experiments (16%), bromide indicated macropore flow, although no *C. parvum* was detected. In only four experiments (7%), bromide falsely indicated no macropore flow given that *C. parvum* was detected. The conditional probability of significant subsurface transport of *C. parvum* (CpBTC = 1) given that the bromide BTC indicated macropore flow (BrBTC = 1) is 78%. Similarly, the conditional probability of observing no significant *C. parvum* (CpBTC = 0) given that the bromide BTC did not indicate macropore flow (BrBTC = 0) is 71%. Therefore, it seems that early breakthrough of a conservative tracer under field conditions is a

Table 5. Final linear mixed-effects regression models† for macropore properties obtained from inverse modeling associated with *C. parvum* effective attenuation rate.

Macropore properties	Regression coefficient for $\Lambda_{\text{eff}20}$ ‡ (SE)	P value§
$\log K_0$	-1.032 (0.256)	0.0024
$\log \theta_0^{\text{CP}}$	1.138 (0.265)	0.0016
Intercept	3.230 (0.576)	0.0002

† Macropore properties were modeled as fixed-effects; experiment (15 randomized sets of two to four soilboxes per experiment) was modeled as a random effect; outcome variable was $\Lambda_{\text{eff}20}$.

‡ $\Lambda_{\text{eff}20}$ obtained from inverse model applied to each experiment.

To obtain the regression coefficients for $\Lambda_{\text{eff}20}$, we considered only experiments for which $\log \theta_0^{\text{CP}} < 0$ and for which the oocyst breakthrough curve (BTC) existed (24 experiments). See Fig. 5b for model validation, and see Table 2 for definition of variables. K_0 : macropore hydraulic conductivity. θ_0^{CP} : macropore water content obtained from oocyst BTC.

§ P value determined from a conditional t test.

strong but not perfect indicator of *C. parvum* transport, at least through relatively shallow soil profiles.

The accuracy of BrBTC as indicator is limited because its classification based on the bromide BTC is subject to estimating matrix flow rates. This estimation depends on knowing the saturated hydraulic conductivity of the soil matrix. The latter is subject

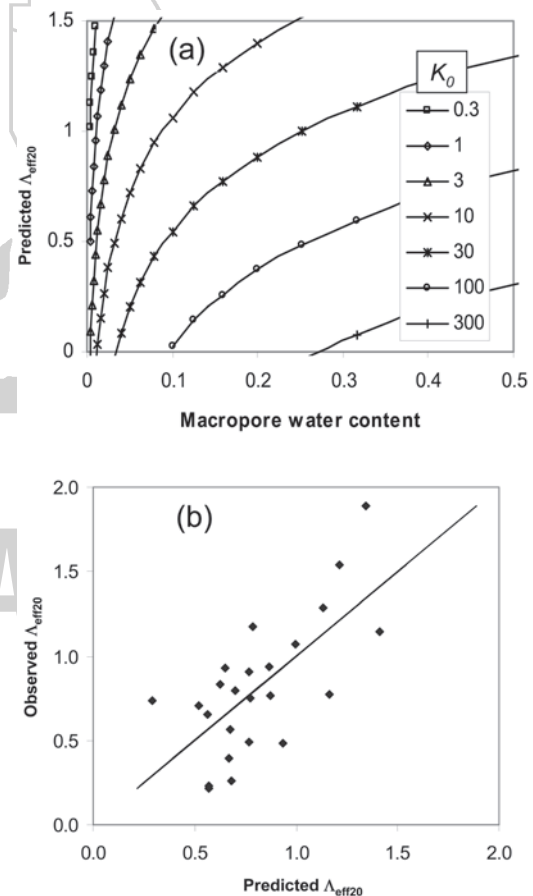


Fig. 5. Linear mixed effects (LME) model predicted oocyst attenuation, $\Lambda_{\text{eff}20}$ (dimensionless), as a function of macropore water content, θ_0^{CP} ($\text{cm}^3 \text{ cm}^{-3}$), and macropore hydraulic conductivity, K_0 (cm d^{-1}). Higher K_0 leads to less attenuation (top). Predicted values are compared with measured values (bottom), yielding a SE of 0.32. Further statistical evaluation of the LME model is given in Table 5.

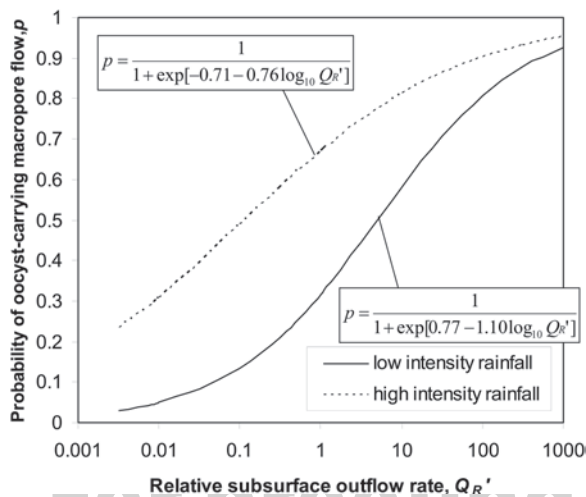


Fig. 6. Logistic regression model showing the risk for oocyst contamination at the 20-cm depth as a function of the ratio of actual subsurface outflow to maximum matrix domain outflow rate.

to spatial variability (between and within soilboxes) and hence uncertainty. Also, estimating matrix flow based on saturated hydraulic conductivity provides only an upper bound (maximum possible rate) for matrix flow and only a conservative estimate of the earliest expected bromide arrival. Hence, classification of BrBTC = 1 indicates a high likelihood of macropore flow (matrix transport cannot explain the early observed BTC), but BrBTC = 0 does not necessarily indicate a low likelihood of macropore flow; it only indicates an absence of fast macropore flow.

The association between CpBTC (a binary indicator) and the measured outflow rate, expressed as Q_r' (a continuous variable), was investigated using logistic regression (e.g., Agresti, 2002; Haan, 2002). We found that the probability of macropore flow with *C. parvum* oocysts, $p(\text{CpBTC} = 1)$, was significantly associated with Q_r' at each of the two rainfall intensities (Fig. 6). The logistic regression indicates that the probability of significant oocyst transport through the soil root zone is 58 and 81% during low rainfall (15 mm h⁻¹) and 81 and 90% during high rainfall

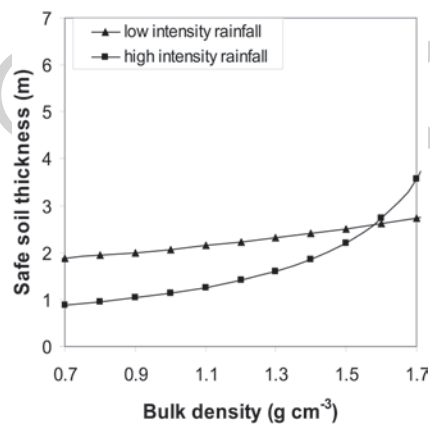


Fig. 7. Soil thickness needed to achieve at least eight orders of magnitude oocyst attenuation. The necessary thickness increases with soil bulk density. At the experimental settings, more soil thickness is needed for protection in low intensity precipitation than in high intensity precipitation.

(40 mm h⁻¹) at Q_r' of 10 and 100, respectively. In contrast, when subsurface outflow rates are equal to the expected saturated matrix flow rate ($Q_r' = 1$), the probability that macropore flow contains *C. parvum* oocysts is less (32% for low rainfall and 67% for high rainfall). More importantly, the logistic regression model suggests that the likelihood of macropore flow with oocysts reduces to insignificant levels (<5%) only when $Q_r' < 1\%$ (i.e., only at very low rainfall and infiltration rates).

Application to Watershed Risk Assessment

Wild and domestic mammalian species have been shown to shed in excess of 10⁶ oocysts per individual per day during the course of an infection (Kuchyzynska and Shelton, 1999; Uga et al., 2000; Atwill et al., 2001). As a result, at the source, oocysts are released from manure into the aqueous solution of soil recharge or runoff at concentrations of 10² to 10³ oocysts mL⁻¹ (Bradford and Schijven, 2002). On the other hand, in humans, the 50% infectious dose of livestock-derived *C. parvum* ranges from 10 to 1000 oocysts (Okhuysen et al., 1999). Considering a typical human consumption of 2 L d⁻¹ and a safety/error factor of 300 to 1000, which is typically used for public health standards, a safe water supply is considered to have less than 10⁻⁵ oocysts mL⁻¹ (<1 oocyst in 100 L). Hence, any buffers between the manure source and the drinking water source must provide an attenuation of at least eight orders of magnitude. In regions with a surficial coarse sand or gravelly aquifer or with a surficial fractured bedrock aquifer, the overlying soil is effectively the main buffer between the oocyst source and the drinking water supply well. To determine how much soil thickness is needed to provide the necessary buffering capacity, we use the LME model of oocyst attenuation, $\Lambda_{\text{eff}20}$ (Table 3, Fig. 4c) to compute the soil thickness, Z , needed to obtain 8 orders of magnitude in oocyst attenuation:

$$Z \text{ [m]} = (8/\Lambda_{\text{eff}20}) \times 0.2 \text{ [m]} \quad [11]$$

With Eq. [11], it can be shown that soil thicknesses on the order of 2 to 5 m are required across a wide range of bulk density to effectively remove oocysts before recharge into groundwater, discharge to surface water, or discharge into tile drains (Fig. 7), even at high-intensity rainfall rates (which seem to be more effective here in removing oocysts; see discussion above). For tile drains, which are typically placed at depths of 1 to 2 m, most soils may therefore provide inadequate protection for *C. parvum* transmission to the tile drain line. In vegetative buffer strips, the soil pathway on hillslopes underneath vegetative buffer strips provides somewhat more protection than the overland flow route, which requires a distance of at least 3 to 10 m for safe removal of oocysts (Fig. 3–5 in Atwill et al., 2002).

In most of the temperate-climate USA, upland and hillslope soils have thicknesses of 0.3 to 2 m and rarely exceed 3 m. By extension of the above analysis, it is, therefore, not unreasonable to argue that, in general, domestic and public water supplies that draw groundwater from surficial fractured, karstic, or gravelly aquifers are at risk for *C. parvum* contamination if some of the pumped water is sufficiently young to allow *C. parvum* oocysts to remain infective. Potentially vulnerable areas include extensive regions in

the mountainous Western USA, in the Appalachian System, in the karstic regions of the Southern and Southeastern United States, and in the formerly glaciated Midwest. Figure 8 shows areas in California with a depth to bedrock of less than 1.52 m (60 inches). Areas vulnerable for *C. parvum* contamination include most of the mountainous areas of California, which typically overlay fractured bedrock often tapped by shallow domestic and small community supply wells. Although such an extension of our laboratory based results must be viewed with caution, it is consistent with watershed studies (e.g., Amirtharajah et al., 2002) and with the significant amount of groundwater samples that have been found contaminated with oocysts, not only in the USA but also in Europe (Lisle and Rose, 1995; Hancock et al., 1998; Moulton-Hancock et al., 2000; Svoboda et al., 1999). Field reconnaissance supports our findings that fractured and dual porosity aquifers, shallow groundwater, and springs are particularly vulnerable to *Cryptosporidium* contamination because soil cover is insufficiently thick for complete removal while it acts as the main attenuation factor (Hancock et al., 1998; Morris and Foster, 2000; Svoboda et al., 1999).

Our results further indicate that aquifers with thick overlying unsaturated zones that contain at least 5 m of loamy sand to loamy clay materials seem to be sufficiently protected from *C. parvum* contamination. Primarily alluvial aquifers with water table depths of 5 to 10 m or more in, for example, the central, southwestern, and western USA are, therefore, less vulnerable to *C. parvum* contamination (e.g., areas in white in Fig. 8). This is consistent with field reconnaissance of *C. parvum* oocysts (e.g., Hancock et al., 1998).

Conclusions

A physically based simple conceptual model of flow and transport in soilbox experiments demonstrates that macropores significantly contribute to soil water flow and the transport of *C. parvum* oocysts. Although oocysts are too large to be transported in the matrix pore space of soils with significant (>10%) fraction of silts and clays, the macropore network in a wide range of soils is sufficiently well developed to transport measurable amounts of oocysts into the subsurface. Understanding macropore flow in soils is therefore critical to assessing the environmental risk of oocyst transport, especially given the very low infectious dose of *C. parvum* needed to initiate human cryptosporidiosis.

This article begins the process of identifying readily measured properties that signal an elevated risk of excessive subsurface transport of pathogens like *C. parvum*. Linear mixed estimation models serve to estimate upscaled macropore properties (hydraulic conductivity, saturation, oocyst attenuation) from readily available soil properties (bulk density) and climate data (rainfall intensity). These can be applied in an upscaled flow and transport model (Eq. [2]–[4]) that may serve as a risk assessment tool. Where direct observation of conservative tracer transport indicates significant macropore flow, a 6 to 90% chance exists that oocysts are transported across a 20-cm-thick soil horizon. Even where macropore flow contributes only a fraction of the total flow, a significant and quantifiable risk for oocyst transport exists. Soils with thicknesses of less than 2 to 3 m are shown to

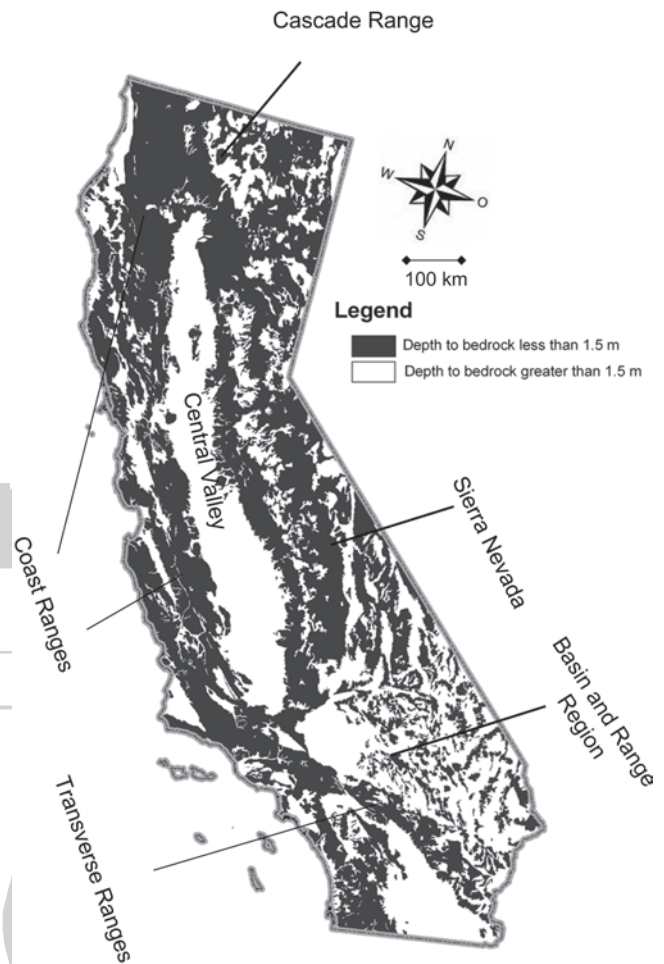


Fig. 8. Spatial extent of soil thickness in California derived from the USDA-NRCS State Soil Geographic Database (STATSGO). Regions identified in black depict areas where the depth to bedrock of dominant soil components of map units is within 1.5 m of the soil surface. Regions in white represent dominant soil components of map units where the depth to bedrock is >1.5 m. (Courtesy of Dr. Anthony T. O'Geen, Dep. Land, Air, and Water Resources, University of California, Davis, CA.)

potentially transmit infectious doses of *C. parvum* oocysts into groundwater supplies. Hence, gravelly, karstic, and fractured rock aquifers may be vulnerable to *C. parvum* contamination across large regions of the USA. More field research is needed to ascertain these field-scale projections of our laboratory findings.

Acknowledgments

This work was supported in part by a grant from the International Life Sciences Institute North America Technical Committee on Food Microbiology. The opinions expressed herein are those of the authors and do not necessarily represent the views of ILSI North America or the committee. The authors express their sincere gratitude for the financial support provided by the Committee for this work. They also thank Dr. Anthony T. O'Geen for providing the soil survey analysis for and preparation of Fig. 8 and Associate Editor Dr. Scott Bradford and two anonymous reviewers for helpful comments and suggestions.

References

- Agresti, A. 2002. Categorical data analysis. John Wiley & Sons, Hoboken, NJ.
- Albrecht, G. 1996. *Cryptosporidium parvum* transport through clay and sand soil columns. B.S. thesis. Cornell Univ., Ithaca, NY.
- Amirtharajah, A., M.H. Young, K.D. Pennell, J.L. Steiner, D.S. Fisher, and D.M. Endale. 2002. Field transport of a *Cryptosporidium* surrogate in small catchments used for grazing lands. Am. Water Works Assoc. Res. Foundation, Report No. 90889. AWWARF, Denver, CO.
- Atwill, E.R. 1996. Assessing the link between rangeland cattle and waterborne *Cryptosporidium parvum* infection in humans. *Rangelands* 182:48–51.
- Atwill, E.R., S. Maldonado Camargo, R. Phillips, L.H. Alonso, K.W. Tate, W.A. Jensen, J. Bennet, S. Little, and T.P. Salmon. 2001. Quantitative shedding of two genotypes of *Cryptosporidium parvum* in California ground squirrels (*Spermophilus beecheyi*). *Appl. Environ. Microbiol.* 67:2840–2843.
- Atwill, E.R., L. Hou, B.M. Karle, T. Harter, K.W. Tate, and R.A. Dahlgren. 2002. Transport of *Cryptosporidium parvum* oocysts through vegetated buffer strips and estimated filtration efficiency. *Appl. Environ. Microbiol.* 68:5517–5527.
- Beven, K., and P. Germann. 1982. Macropores and water flow in soils. *Water Resour. Res.* 18:1311–1325.
- Bicudo, J.R., and S.M. Goyal. 2003. Pathogens and manure management systems: A review. *Environ. Technol.* 24:115–130.
- Bradford, S.A., and M. Bettahar. 2005. Straining, attachment, and detachment of *Cryptosporidium* oocysts in saturated porous media. *J. Environ. Qual.* 34:469–478.
- Bradford, S.A., and J. Schijven. 2002. Release of *Cryptosporidium* and *Giardia* from dairy calf manure: Impact of solution salinity. *Environ. Sci. Technol.* 36:3916–3923.
- Bradford, S.A., J. Simunek, M. Bettahar, M.Th. Van Genuchten, and S.R. Yates. 2003. Modeling colloid attachment, straining, and exclusion in saturated porous media. *Environ. Sci. Technol.* 37:2242–2250.
- Brush, C.F., W.C. Ghiorse, L.J. Anguish, J.-Y. Parlange, and H.G. Grimes. 1999. Transport of *Cryptosporidium parvum* oocysts through saturated columns. *J. Environ. Qual.* 28:809–815.
- Darnault, C.J.G., P. Garnier, Y.J. Kim, K. Oveson, T.S. Steenhuis, J.-Y. Parlange, M. Jenkins, W.C. Ghiorse, and P.C. Baveye. 2003. Preferential transport of *Cryptosporidium parvum* oocysts in variably-saturated subsurface environments. *Water Environ. Res.* 75:113–120.
- Darnault, C.J.G., T.S. Steenhuis, Y.J. Kim, P. Garnier, M. Jenkins, W.C. Ghiorse, P.C. Baveye, and J.-Y. Parlange. 2004. Preferential flow and the transport of *Cryptosporidium parvum* oocysts through the vadose zone: Experiments and modeling. *Vadose Zone J.* 3:262–270.
- De Carvalho, G., R.E. Mara Prioli Ciapina, R.S. Espindola, A. Pacheco, and V. Helena Pellizari. 2000. Detection of *Cryptosporidium parvum* sp. oocysts in groundwater for human consumption in Itaquaquecetuba City, Sao Paulo-Brazil. *Braz. J. Microbiol.* 31:151–153.
- Ginn, T., B.D. Wood, K.E. Nelson, T.D. Scheibe, E.M. Murphy, and T. Prabhakar Clement. 2002. Processes in microbial transport in the natural subsurface. *Adv. Water Resour.* 25:1017–1042.
- Haan, C.T. 2002. Statistical methods in hydrology, 2nd ed. Iowa State Press, Ames, IA.
- Hancock, C.M., J.B. Rose, and M. Callahan. 1998. *Crypto* and *Giardia* in U.S. groundwater. *J. Am. Water Works Assoc.* 90:58–61.
- Harter, T., S. Wagner, and E.R. Atwill. 2000. Colloid transport and filtration of *Cryptosporidium parvum* in sandy soils and aquifer sediments. *Environ. Sci. Technol.* 34:62–70.
- Hillel, D. 2004. Introduction to environmental soil physics. Academic Press, San Diego, CA.
- Kirkham, M.B. 2005. Principles of soil and plant water relations. Elsevier Academic Press, Burlington, MA.
- Kuchzynska, E., and D.R. Shelton. 1999. Method for detection and enumeration of *Cryptosporidium parvum* oocysts in feces, manures, and soils. *Appl. Environ. Microbiol.* 65:2820–2826.
- Lisle, J.T., and J.B. Rose. 1995. *Cryptosporidium* contamination of water in the USA and UK: A mini review. *J. Water Supply Res. Technol. Aqua* 44:103–117.
- Marly, X., S. Chevalier, M. Bues, J. Schwartzbrod, and O. Estevenon. 2001. Experimental investigations and numerical modelling of *Cryptosporidium parvum* transport behaviour in aquifers. *Water Sci. Technol.* 43:109–116.
- Mawdsley, J.L., A.E. Brooks, and R.J. Merry. 1996a. Movement of the protozoan pathogen *Cryptosporidium parvum* in three contrasting soil types. *Biol. Fertil. Soils* 21:30–36.
- Mawdsley, J.L., A.E. Brooks, R.J. Merry, and B.F. Pain. 1996b. Use of a novel soil tilting table apparatus to demonstrate the horizontal and vertical movement of the protozoan pathogen *Cryptosporidium parvum* in soil. *Biol. Fertil. Soils* 23:215–220.
- McDonald, M.G., and A.W. Harbaugh. 1988. A modular three-dimensional finite-difference ground-water flow model. U.S. Geological Survey Techniques of Water-Resources Investigations, Book 6, chap. A1. USGS, Reston, VA.
- McDowell-Boyer, L.M., J.R. Hunt, and N. Sitar. 1986. Particle transport through porous media. *Water Resour. Res.* 22:1901–1902.
- McGechan, M.B., and D.R. Lewis. 2002. Transport of particulate and colloid-sorbed contaminants through soils, Part I: General principles. *Biosyst. Eng.* 83:255–273.
- Messing, I., A. Alriksson, and W. Johansson. 1997. Soil physical properties of afforested and arable land. *Soil Use Manage.* 13:209–217.
- Messner, M.J., and R.L. Wolpert. 2000. Occurrence of *Cryptosporidium* in the nation's drinking water sources—ICR data analysis. In Proceedings, Water Quality Technology Conf. Salt Lake City, UT. 5–9 Nov. 2000. American Water Works Assoc., Denver, CO.
- Minasny, B., J.W. Hopmans, T. Harter, S.O. Eching, A. Tuli, and M.A. Denton. 2004. Neural networks prediction of soil hydraulic functions for alluvial soils using multistep outflow data. *Soil Sci. Soc. Am. J.* 68:417–429.
- Mori, Y., T. Maruyama, and T. Mitsuno. 1999a. Soft x-ray radiography of drainage patterns of structured soils. *Soil Sci. Soc. Am. J.* 63:733–740.
- Mori, Y., K. Iwama, T. Maruyama, and T. Mitsuno. 1999b. Discriminating the influence of soil texture and management-induced changes in macropore flow using soft X-rays. *Soil Sci.* 164:467–482.
- Morris, B.L., and S.S.D. Foster. 2000. *Cryptosporidium* contamination hazard assessment and risk management for British groundwater sources. *Water Sci. Technol.* 41:67–77.
- Moulton-Hancock, C., J.B. Rose, G.J. Vasconcelos, S.I. Harris, P.T. Klonicki, and G.D. Sturbaum. 2000. *Giardia* and *Cryptosporidium* occurrence in groundwater. *J. Am. Water Works Assoc.* 92:117–123.
- Okhuysen, P.C., C.L. Chappell, J.H. Crabb, C.R. Sterling, and H.L. DuPont. 1999. Virulence of three different *Cryptosporidium parvum* isolates for healthy adults. *J. Infect. Dis.* 180:1275–1281.
- Pinheiro, J.C., and D.M. Bates. 2000. Mixed effects model in S and S-Plus. Springer, New York.
- Poulsen, T.G., P. Moldrup, L.W. De Jonge, and T. Komatsu. 2006. Colloid and bromide transport in undisturbed soil columns: Application of two-region model. *Vadose Zone J.* 5:649–656.
- Rose, J.B., C.P. Gerba, and W. Jakubowski. 1991. Survey of potable water supplies for *Cryptosporidium* and *Giardia*. *Environ. Sci. Technol.* 25:1393–1400.
- Searcy, K.E., A. Packman, E.R. Atwill, and T. Harter. 2005. Association of *Cryptosporidium parvum* with suspended particles: Impact on oocyst sedimentation. *Appl. Environ. Microbiol.* 71:1072–1078.
- Shirmohammadi, A., H. Montas, L. Bergström, A. Sadeghi, and D. Bosch. 2005. Preferential flow: Identification and quantification. p. 289–308. In J. Álvarez-Benedí and R. Muñoz-Carpena (ed.) Soil-water-solute process characterization: An integrated approach. CRC Press, Boca Raton, FL.
- Svoboda, P., S. Ruchti, C. Bissegger, and M. Tanner. 1999. Occurrence of *Cryptosporidium* spp. oocysts in surface, raw and drinking water samples. Publications Kantonales Labor, Kanton Basel-Landschaft. Available at <http://www.baseland.ch/docs/vsd/labor/aktuell/publ/crypto.htm> (verified 11 June 2007).
- Uga, S., J. Matsuo, E. Kono, K. Kimura, M. Inoue, S.K. Rai, and K. Ono. 2000. Prevalence of *Cryptosporidium parvum* infection and pattern of oocyst shedding in calves in Japan. *Vet. Parasitol.* 94:27–32.
- Walker, M.J., C.D. Montemagno, and M.B. Jenkins. 1998. Source water assessment and nonpoint sources of acute toxic contaminants: A review of research related to survival and transport of *Cryptosporidium parvum*. *Water Resour. Res.* 34:3383–3392.
- Walker, F.R., and J.R. Stedinger. 1999. Fate and transport model of *Cryptosporidium*. *J. Environ. Eng.* 125:325–333.
- Zevi, Y., A. Dathe, J.F. McCarthy, B.K. Richards, and T.S. Steenhuis. 2005. Distribution of colloid particles onto interfaces in partially saturated sand. *Environ. Sci. Technol.* 39:7055–7064.
- Zheng, C., and P.P. Wang. 1999. MT3DMS: A modular three-dimensional multi-species transport model for simulation of advection, dispersion, and chemical reactions of contaminants in groundwater systems; documentation and user's guide. U.S. Army Engineer Research and Development Center Contract Report SERDP-99-1. USACE, Vicksburg, MS.